

2D phononic crystals: Disorder matters

Markus R. Wagner,^{1,*} Bartłomiej Graczykowski,¹ Juan Sebastian Reparaz,¹ Alexandros El Sachat,^{1,2} Marianna Sledzinska,¹ Francesc Alzina,¹ and Clivia M. Sotomayor Torres^{1,3}

¹*Catalan Institute of Nanoscience and Nanotechnology (ICN2),
CSIC and The Barcelona Institute of Science and Technology,
Campus UAB, Bellaterra, 08193 Barcelona, Spain*

²*Dept. of Physics, Universitat Autònoma de Barcelona,
08193 Bellaterra (Barcelona), Spain*

³*ICREA - Catalan Institute for Research and Advanced Studies, 08010 Barcelona, Spain*

(Dated: June 4, 2019)

Abstract

The design and fabrication of phononic crystals (PnCs) hold the key to control the propagation of heat and sound at the nanoscale. However, there is a lack of experimental studies addressing the impact of order / disorder on the phononic properties of PnCs. Here, we present the first comparative investigation of the influence of disorder on the hypersonic and thermal properties of 2-dimensional PnCs. PnCs of ordered and disordered lattices were fabricated of circular holes with equal filling fractions in free-standing Si membranes. Ultrafast pump and probe spectroscopy (asynchronous optical sampling) and Raman thermometry based on a novel two-laser approach are used to study the phononic properties in the GHz and THz regime, respectively. Finite element method simulations of the dispersion relation and 3-dimensional displacement fields furthermore enable the unique identification of the different hypersonic vibrations. The introduction of short range disorder is shown to modify the phonon dispersion and coherence in the hypersonic (GHz) range without affecting the room temperature thermal conductivity.

PACS numbers: 63.22.-m, 78.47.J-, 78.47.jg, 82.53.Mj, 02.70.Dh

Keywords: phononic crystals, order, disorder, coherent acoustic phonons, thermal conductivity, asynchronous optical sampling, Raman thermometry, finite element method

INTRODUCTION

Phononic crystals (PnCs), the acoustic analogues of the more established photonic crystals, constitute an attractive class of materials with the potential to manipulate and control the propagation of vibrational energy, i.e., sound and heat. Caused by their periodic structure, these materials can exhibit complete acoustic band gaps due to Bragg reflections and local resonances controlled by geometry and material properties [1–5]. The periodic modulation of their elastic properties [2, 3, 6–10] and the reduced dimensionality in nanostructures [11–13] lead to strong modifications of the acoustic phonon dispersion which directly affects the phonon group velocity, phonon propagation, and, ultimately, sound and heat transport.

The continuing miniaturization and progress in nanofabrication techniques has enabled the reduction of the characteristic sizes of PnCs to the nanometer scale and thereby allows the modification and control of phonon propagation and transport properties in the frequency range from hypersonic (GHz) phonons [7–10] to nanoscale thermal transport governed mainly by THz phonons [5, 14–19]. The prospect to tailor the thermal conduction and heat capacity has recently triggered tremendous research activities and several works have reported the successful reduction of the room temperature thermal conductivity in PnCs impacting potential applications in thermoelectricity [14, 15, 20–24]. The ability to modify the phonon dispersion relation in the hypersonic frequency range, and thus the group velocity of acoustic phonons, has paved the way to applications in RF communication technologies [25] and optomechanics [26–28]. However, studies of the GHz phonon dispersion relation have been performed mostly for bulk [3, 7, 8, 29–31] and surface PnCs [9, 32, 33], whereas the effects of hole patterning and pillar growth in combination with second order periodicity in thin membranes was only recently studied [10]. In particular, the concept of disorder, a key aspect in the design of modern photonics [34] for the guidance and trapping of light and ultrasound by Anderson localization [35–39], is almost completely unexplored in phononic crystals to the present day.

In this work, we investigate the influence of short-range disorder in Si membrane-based 2D phononic crystals on the GHz and THz phononic properties. We use time-resolved femtosecond pump-probe spectroscopy based on asynchronous optical sampling (ASOPS) as a novel approach to measure the zone-center phonon spectrum and phonon dynamics

in the time domain. Finite element method (FEM) simulations are used to calculate the dispersion relation, 3D displacement fields, and amplitudes of the different modes. The thermal conductivity of the ordered and disordered PnCs is measured by the novel contactless technique of 2-laser Raman thermometry, here applied to PnCs for the first time.

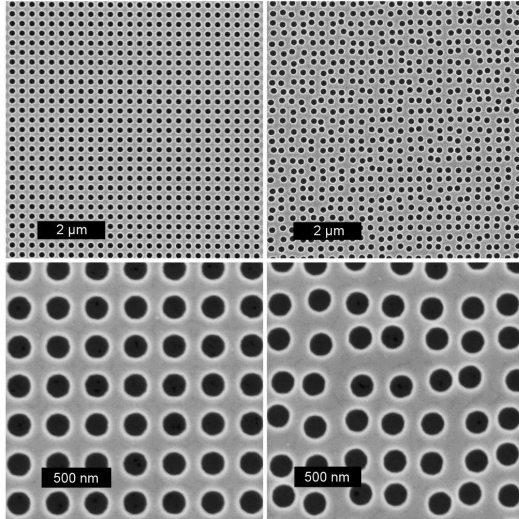


FIG. 1. Scanning electron microscope images of Si membrane based 2D phononic crystals with a thickness of 250 nm. Left: ordered PnC with hole diameter of 175 nm and pitch of 300 nm, filling fraction $\phi = 0.267$, right: disordered PnC with equal hole diameter and filling fraction and 20% disorder.

RESULTS AND DISCUSSION

2D phononic crystals were fabricated of free-standing silicon membranes using electron beam lithography and reactive ion etching to generate ordered and disordered hole patterns with equal filling fractions (Fig.1) [40]. The disorder was introduced by random displacement in the x and y directions within the unit cell of the PnC lattice with an average disorder of 20%. The acoustic phonon dynamics of the ordered and disordered PnCs with the same filling fractions were investigated using femtosecond pump-probe reflectivity measurements using asynchronous optical sampling (ASOPS) [41–43] (see section Methods for details). Fig. 2 shows a typical transient for a 250 nm thick Si membrane before PnC patterning. The initial intense peak originates from the electronic excitation of the material followed by

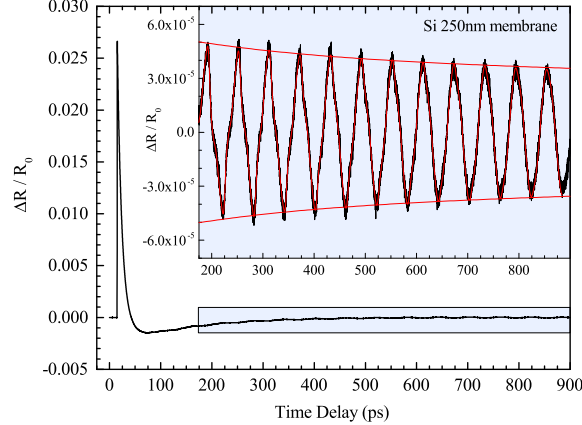


FIG. 2. (Color online) Time-resolved intensity modulation of the reflected probe beam $\Delta R/R_0$. Inset: Reflectivity modulation after subtraction of the electronic contribution and system response correction. Note the change in the y-scale.

carrier relaxation with electron and hole relaxation times and LO phonon lifetimes of several hundreds of femtoseconds to about 2 ps [44, 45]. The optical excitation of acoustic vibrations arises from the electronic and thermal stresses induced by the pump pulse which are determined by the generated electron-hole pair density and the temperature-induced lattice deformation, respectively [42, 46, 47]. The excited out-of-plane (dilatational) oscillations change the optical cavity thickness of the membrane which leads to a modulation of the probed reflectivity by the Fabry-Perot effect. The inset of Fig. 2 displays the time-resolved intensity modulation of the reflected probe laser after subtraction of the electronic contribution and system response correction. The resulting signal resembles a saw-tooth like shape in the beginning of the time trace but changes to a sinusoidal pattern towards the end of the transient. This behavior is explained considering different acoustic phonon lifetimes as discussed below.

The frequencies of the acoustic phonon modes can be derived from numerical Fourier transformation as shown in the center panel of Fig. 3(a). The different harmonics in the vibrational spectrum of the membrane appear as equidistant peaks as a consequence of the confinement of the acoustic modes [11, 42, 48]. The lowest frequency peak at 16.8 GHz thereby corresponds to the first order symmetric (S_1) mode. In addition, modes up to the 9th harmonic at 151 GHz are clearly visible in the frequency spectrum. The decreasing

amplitude of the higher harmonics can be accurately described by Eq. 2 which in the case of the unpatterned membranes simplifies to a $1/\omega^2$ relation [42]. The absence of even harmonics can be understood taking into account that these modes have only in-plane displacement at the Γ point so that no modulation of the optical cavity thickness occurs [42, 49]. Using the value of the longitudinal sound velocity for Si [001] of $v_L = 8433 \text{ m/s}$ [50], the frequencies of the observed modes provide a direct measurement of the membrane thickness given by $d = nv_L/2f_n$, where f_n is the frequency of the n -th harmonic ($n = 1, 3, 5, \dots$) of the symmetric (dilatational) mode [42]. The so derived frequencies of the first and higher order modes can be used as input parameters for a multi damped-sinusoidal fit of the transient as shown in the inset of Fig. 2 and Fig. 3(a). Following this approach, decay times of about 6 ns for the fundamental mode and 300-400 ps for the third and fifth harmonics are obtained. The significantly shorter lifetime of the higher harmonics is directly visible in the transient by the disappearance of the saw-tooth pattern for larger time delays. It can be explained considering that the coherent phonon lifetimes of the higher harmonics exhibit a pronounced frequency dependence with strongly reduced lifetimes for higher frequency modes [49].

In the case of the S_1 mode, we find a good agreement of the measured lifetime of 6 ns for the 250 nm thick Si membrane with previous studies of the acoustic phonon dynamics as function of membrane thickness [51], picosecond ultrasonic experiments of bulk Si in a comparable frequency range [52, 53] and the determination of the lower lifetime limit of 9 ns in a 222 nm thick membrane using subharmonic resonance profile analysis [43]. In addition to the first and higher order dilatational modes, another signal is observed in the FFT spectrum at 23.8 GHz with a lifetime of about 200 ps. The intensity of this mode as compared to the S_1 mode at 16.8 GHz is rather weak with an amplitude ratio of about 0.03 (right panel of Fig. 3). Using FEM modeling, we identify this mode as the symmetric S_2 mode which might be visible due to excitation of propagating in-plane modes with small but nonzero wave numbers and therefore nonzero out-of-plane displacement [54].

Following the discussion of the acoustic phonon dynamics of the non-patterned membrane, we now focus on the modification of the frequency spectrum in ordered and disordered membrane based PnCs by hole patterning of the original membrane. The time resolved pump-probe reflectivity spectra for the ordered and disordered PnCs are displayed in the left panel of Fig. 3 (b) and (c). Apparently, the sawtooth and sinusoidal signal of the unpatterned membrane in Fig. 3(a) is replaced by a more complex time response of the

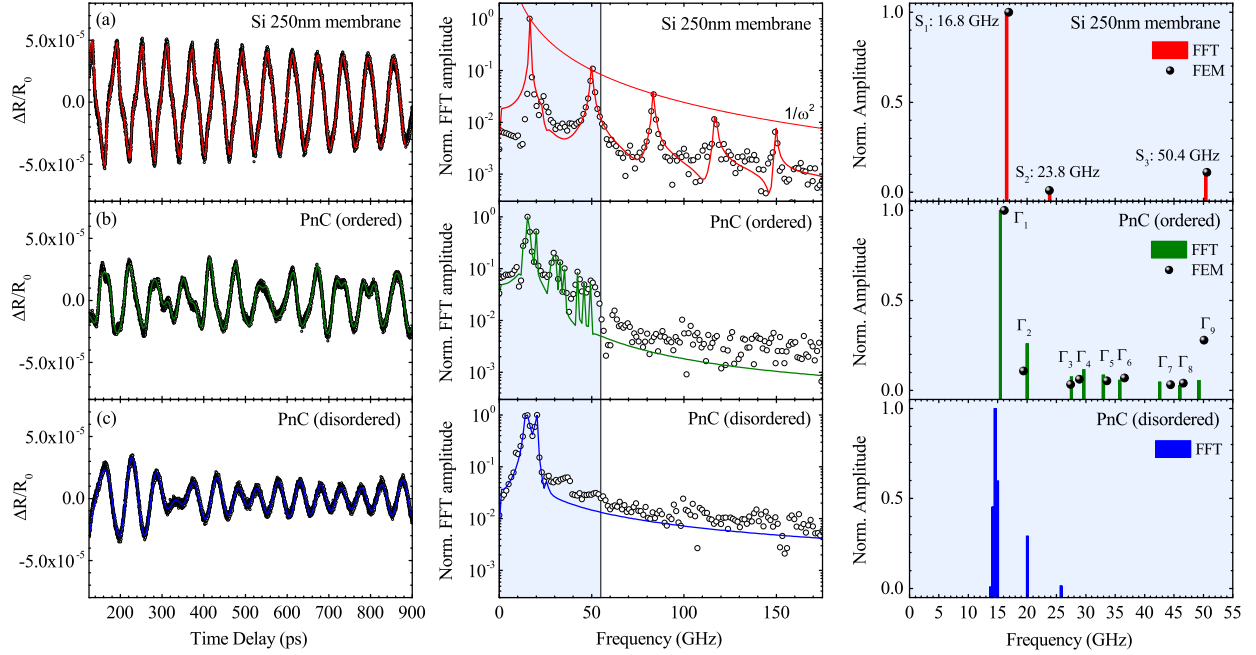


FIG. 3. (Color online) Left: Time-resolved reflectivity spectra and corresponding damped sinusoidal fits of (a) unstructured Si membrane, (b) ordered phononic crystals, (c) disordered phononic crystal. Center: Fourier transformation of measured and fitted time-resolved reflectivity spectra. Right: Normalized amplitude and acoustic phonon frequencies as obtained by FFT of time resolved reflectivity spectra (bars) and finite element method calculations (dots).

reflectivity change in the ordered and disordered PnCs. This indicates a strong modification of the phonon dispersion relation with the appearance of additional acoustic phonon modes that contribute to reflectivity modulations. The frequency spectra as determined by FFT of the time-domain signals are displayed in the center panel of Fig. 3. Using this approach, one can directly obtain the complete zone-center phonon frequency spectrum up to the THz regime. However, we focus here on the range between 0 and 55 GHz, as most of the modes with relevant amplitude for 250 nm thick membrane based PnCs are found in this frequency band. The relative amplitudes of the different modes, normalized to the most intense mode at about 16 GHz, are displayed in the right panel of Fig. 3 and compared to the results of FEM simulations (black dots). For the unpatterned membrane, the first three symmetric modes S_1 , S_2 , and S_3 are observed and perfectly reproduced by the FEM simulations regarding both amplitude and frequency of the modes. In the case of the ordered PnCs, nine discrete

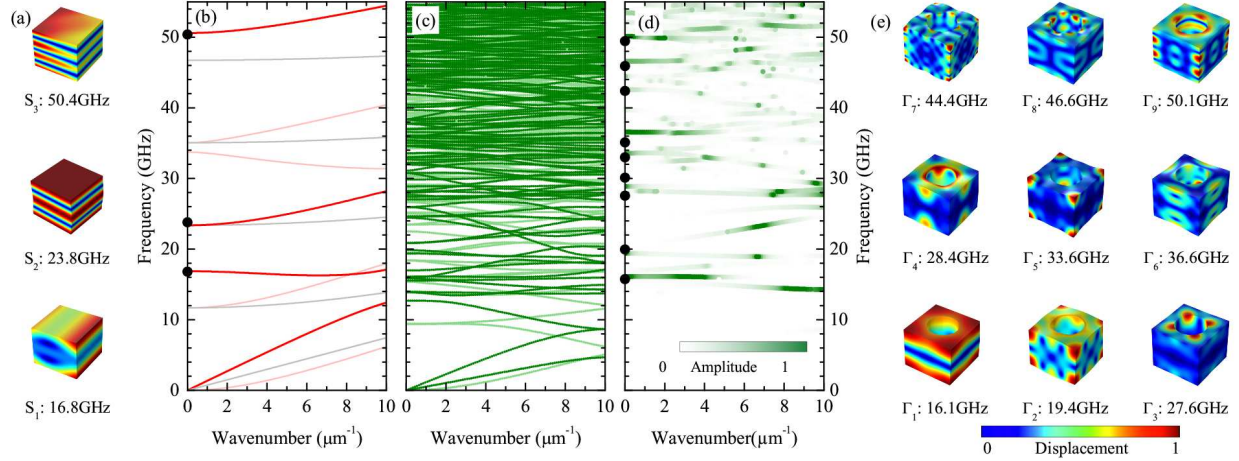


FIG. 4. (Color online) Calculated acoustic phonon dispersion relation for a 250 nm thick Si membrane without pattern in $[110]$ direction (b) and with ordered hole pattern in ΓX direction (2D PnC) (c) showing symmetric (dark color), antisymmetric (light color) and shear horizontal (gray) modes. Dispersion relation displaying the amplitude of the out-of-plane modes in ordered PnCs (d). Black dots indicate the experimentally obtained zone-center phonon frequencies (b) and (d). The corresponding 3D displacements fields for the symmetric modes at the Γ point are shown for the unpatterned membrane (a) and the ordered PnC (e). Only modes with non-vanishing out-of-plane displacement are displayed.

zone-center modes ($\Gamma_1 - \Gamma_9$) can be clearly distinguished in good agreement with the FEM calculations. However, this is not the case in the disordered PnCs as will be discussed in more detail below.

In order to explain the observed differences between the unpatterned membrane and the ordered PnC, we calculate the dispersion relation and the 3-dimensional displacement fields for the zone-center modes up to 55 GHz (Fig 4). The dispersion relations for the membrane before and after hole patterning are displayed in Fig. 4(b) and Fig. 4(c), respectively. The strong modifications and the appearance of additional modes in the 2D PnC compared to the reference sample arises from band folding and band splitting when the Bragg condition is satisfied [10]. Considering the multitude of different modes in the dispersion relation of the ordered PnC in Fig 4(c), the question arises as to why are there only nine discrete modes visible in the time domain measurements in this frequency range. The answer becomes clear,

if one considers the amplitudes of the measured out-of-plane displacement of the different modes according to Eq. 2 which are plotted together with the measured zone-center phonon frequencies in Fig 4(d). In excellent agreement with the experimental results, the calculations reveal nine discrete modes between 15 GHz and 51 GHz with non-vanishing out-of-plane displacement amplitude at the Γ point ($\Gamma_1 - \Gamma_9$) as compared to three modes ($S_1 - S_3$) in the unpatterned membrane (Fig. 4(b)). The corresponding 3-dimensional displacement fields for these modes are displayed in Figs. 4 (a) and (e) and thereby enable the unique identification of the displacement characteristic of each of the observed modes.

Comparing the discussed acoustic phonon spectrum of the ordered PnCs with those of the disordered PnCs, it is apparent that the dispersion relation and zone-center phonon frequencies are significantly different from each other. As most prominent feature, no individual modes above about 25 GHz can be resolved (see center and right panel of Fig. 3(c)). This observation demonstrates the importance of translational symmetry to build complex high frequency modes. In a disordered PnC, the individual modes can locally differ in energy and dispersion resulting in the obliteration of discrete modes. In conjunction with the small out-of-plane displacement amplitudes of higher frequency modes even in the ordered PnCs (c.f. Fig. 4(e)), the missing periodicity in the disordered PnCs prevents the formation and detection of individual high frequency modes in the hypersonic frequency regime. On the other hand, it is interesting to note that there are still two modes visible in the disordered PnCs with low frequencies of about 15 GHz and 20 GHz which are comparable in frequency and amplitude to the Γ_1 and Γ_2 modes of the ordered PnC, although significantly broadened. The fact that these modes are largely unaffected by disorder can be understood by a comparison of the 3D displacement fields of the lowest frequency modes in the unpatterned membrane (S_1) and the ordered PnC (Γ_1) in Figs. 4(a) and 4(e), respectively. Obviously, both modes exhibit a large out of plane displacement amplitude and similar displacement symmetry indicating that they are mainly governed by the bare membrane and do not depend on the second-order periodicity. Consequently, these modes are not significantly affected by the degree of order / disorder in the PnCs. Finally, it should be noted that the frequency of the lowest energy mode in the disordered PnC (14.6 GHz) and ordered PnC (15.5 GHz) is smaller as compared to the reference membrane (16.8 GHz) which is caused by the softening of the material due to the porosity in the PnC and results in a frequency down shift of this mode.

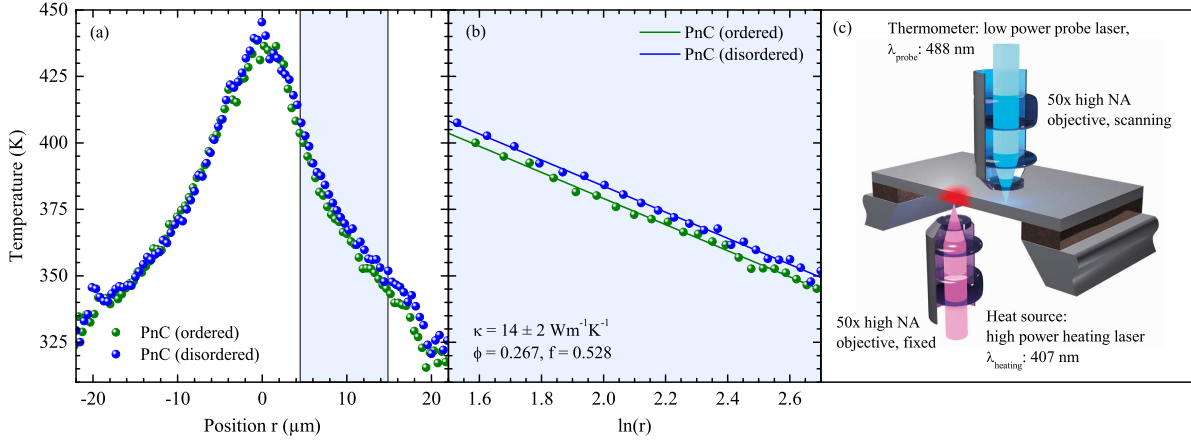


FIG. 5. (Color online) Temperature line-scan profiles of the order and disordered PnCs upon a localized thermal excitation using two-laser Raman thermometry (2LRT) (a). Thermal conductivity derived using a 2-dimensional heat transport model considering a filling fraction of $\phi = 0.267$ (b). Schematic illustration of the experimental concept of the 2LRT technique (c).

Up to this point, we have limited our discussion to the hypersonic (GHz) frequency range of the phonon spectrum which was shown to be highly sensitive to disorder in the PnCs. Taking into account that no discrete phonon modes in the disordered PnCs could be observed at frequencies above 25 GHz, it is clear that a different approach is required to investigate the influence of order and disorder on the thermal properties of the phononic crystals. For this purpose we have developed a contactless technique suitable to investigate the thermal conductivity of 2D structures, namely 2-laser Raman thermometry (2LRT) [55]. The main advantage of this technique with respect to established ones, such as electrical measurements on suspended structures or time-domain thermoreflectance (TDTR), is that no thermal interface resistances are present due to its contactless fashion. Thus, the thermal conductivity of the PnCs can be accurately obtained without the need of any modeling. A spatially fixed heating laser generates a localized steady-state thermal excitation, whereas a low power probe laser measures the spatially resolved temperature profile through the temperature dependent Raman effect. In this particular case, the spectral position of the Si zone center optical phonon was used as temperature sensor. Further details about the methodology can be found in Ref. [[55]]. Fig. 5(a) displays the temperature profiles for

ordered and disordered PnCs as obtained by 2LRT with the experimental arrangement shown schematically in Fig. 5(c). Applying Fourier’s law in 2-dimensions for a thermally isotropic medium leads to a temperature field $T(r)$ with

$$T(r) = T_0 + \frac{P_{abs}}{2\pi f d \kappa_0} \ln(r/r_0) \quad (1)$$

where (r_0, T_0) is an arbitrary point in the temperature field, P_{abs} is the absorbed power, $\phi = 0.267$ is the filling fraction which accounts for the missing material in the holes forming the PnC, $f = 0.528$ is the corresponding correction factor [22], d is the thickness of the PnC membranes, and κ_0 is the thermal conductivity. Here, κ_0 can be treated as temperature independent since the studied temperature range is sufficiently small (≈ 100 K). Fig. 5(b) displays the thermal decays in logarithmic scale according to Eq. 1, thus, the slope of the thermal decay in Fig. 5(b) is directly related to κ_0 . Based on these measurements, we obtain the same value for the thermal conductivity $\kappa_0 = 14 \pm 2 \text{ Wm}^{-1}\text{K}^{-1}$ for the ordered and disordered PnCs as compared to $\kappa_0 = 80 \pm 3 \text{ Wm}^{-1}\text{K}^{-1}$ in case of the unpatterned membrane [55]. The reduction in the thermal conductivity of the PnCs to 17.5% of the value of the unpatterned membrane (about 6-fold reduction) is in accordance with other recent studies of the thermal conductivity in PnCs with comparable dimensions [14, 15, 20, 22–24]. It cannot solely be explained by the mass loss due to hole patterning (porosity effect) but is typically attributed to an increase of boundary scattering by the introduction of holes as well as coherent effects resulting in a modification of the dispersion relation and ultimately a reduction in thermal conductivity [14, 15, 22, 23]. However, it should be noted that the precise contributions of coherent effects and boundary scattering are still a subject of active debate and scientific research [15, 17, 22].

More important for the current work is the fact that there is no significant influence of disorder on the thermal phonons in the THz range as demonstrated by the same thermal conductivity of ordered and disordered PnCs despite the strong modification of the phononic properties in the hypersonic frequency range. A possible explanation can be given considering that the frequency range of thermal phonons at room temperature are in the THz range which implies phonon wavelengths below 10 nm in contrast to the typical dimensions of the studied samples (≈ 100 nm). It is thus possible to use disorder to modify phononic properties only in specific frequency bands, here, in the hypersonic range, while preserving the same thermal conductivity. In a similar manner, it is conceivable to achieve a tuning of

thermal properties by changing the degree of disorder in smaller structures with comparable dimensions to the wavelengths of thermal phonons.

CONCLUSIONS

In summary, we have addressed the question to what extent disorder influences the phononic properties of 2-dimensional phononic crystals both in the GHz and THz frequency range. In a first step, we have shown that short range order has a large impact on the hypersonic vibrations of the PnCs as measured by femtosecond time domain spectroscopy. Using finite element method simulations we have uniquely identified the displacement characteristic of each mode by the calculation of the dispersion relation and the 3-dimensional displacement fields. The introduction of disorder in the PnCs was shown to drastically modify the hypersonic phonon properties resulting in the obliteration of higher frequency modes in the GHz range. On the other hand, the influence of order and disorder in PnCs on the thermal phonons in the THz regime was studied indirectly by measuring the thermal conductivity using 2-laser Raman thermometry. Upon hole patterning, a 6-fold reduction of the thermal conductivity was observed for the ordered and disorderd PnCs ($\kappa_0 = 14 \pm 2 \text{ Wm}^{-1}\text{K}^{-1}$) as compared to the unpatterned membrane ($\kappa_0 = 80 \pm 3 \text{ Wm}^{-1}\text{K}^{-1}$). The disorder in the PnCs proved to be without consequence for the thermal conductivity of the PnCs. The presented results might therefore open a possible way for the controlled usage of disorder to modify the phononic properties, e.g. sound or heat transport, in a certain range of the phononic spectrum while maintaining acoustic or thermal properties governed by phonons in different ranges of the frequency spectrum.

METHODS

Commercially available single crystalline silicon (100) membranes (Norcada Inc.) with a thickness of 250 nm and window size of 3.2x3.2 mm² were used as basis for the fabrication of the 2D PnCs [40]. PMMA 950k (Allresist) was spun at 4000 rpm for one minute, followed by 60 min bake at 100°C in an oven. Electron beam lithography (Raith 150-TWO) was performed to define ordered and disordered PnCs with a hole size of 175 nm and a pitch of 300 nm for the ordered PnCs and equal filling fraction for the disordered PnCs (c.f. Fig. 1).

The dimensions of the structures were $50 \times 50 \mu\text{m}$. After development in 1:3 methyl isobutyl ketone:isopropanol (MIBK:IPA), the samples were post-baked for 1 min in 80°C on a hot plate. The pattern was transferred to silicon using the Bosch process (Alcatel AMS-110DE) and the final samples were cleaned in an oxygen plasma system (PVA Tepla).

The acoustic phonon dynamics in the GHz range were investigated using femtosecond pump-probe reflectivity measurements based on the asynchronous optical sampling (ASOPS) technique [41–43]. The method is based on two asynchronously coupled Ti:sapphire ring cavity lasers with a repetition rate of 1 GHz and a nominal pulse length of about 50 fs. The time delay between the pump and probe pulses is achieved through an actively stabilized frequency offset of 10 kHz between the repetition rate of the two laser oscillators. This allows for a linearly increasing time delay between pump and probe pulses with steps of 10 fs without the need for a mechanical delay line. Owing to the high repetition rate of 1 GHz, an excellent signal-to-noise ratio of above 10^7 can be achieved for typical acquisition times in the seconds to minutes range. Pump-probe reflectivity measurements were performed by focusing both lasers collinear onto the PnC membranes using a 50x microscopy objective (Olympus, NA = 0.50) in normal incidence geometry, resulting in a spot size of about $2 \mu\text{m}$ which corresponds to an excitation area in the PnC of about 35 unit cells. The pump laser was tuned to a center wavelength of 770 nm with an average power of 8 mW and the probe laser to 830 nm with a power of 4 mW. The reflected probe laser was spectrally filtered by a long-pass filter at 800 nm to eliminate any contribution from the pump laser and recorded with a low noise photodetector of 125 MHz bandwidth.

The acoustic phonon band diagrams, 3D displacement fields and relative changes of reflectivity corresponding to particular mechanical modes were calculated by means of FEM modeling as described in Ref. [10]. In principle the reflectivity of the membrane is modulated by the induced mechanical modes which result in non-zero average thickness variations. Here the model assumes a predominant role of the optical cavity thickness (OCT) mechanism with negligible contribution of the photoelastic effect (PE) [42]. The pump induced variation of the membrane thickness Δd is of the order of a pm and directly proportional to the measured relative change of the reflectivity $\Delta R/R_0$. In the case of the PnCs the mechanical modes are complex and Δd is position dependent. We correlate the amplitudes A_i of the modes ω_i with their corresponding average change of thickness $|\overline{\Delta d}|$ calculated over the whole FEM unit cell using the formula:

$$A_i(\omega_i) \propto \overline{\Delta d} \propto \frac{1}{S\omega_i} \int_S ((u_i(z=0) - u_i(z=d)))dS, \quad (2)$$

where $u_i(z)$ are the out-of-plane displacement components, and S is the free surface area. The displacement fields of all the FEM solutions are normalized in such a way that all the modes store the same elastic energy and are populated according to the Planck distribution at high temperature.

ACKNOWLEDGMENTS

The authors acknowledge financial support from the EU FP7 project MERGING (Grant No. 309150), NANO-RF (Grant No. 318352) and QUANTIHEAT (Grant No. 604668); the Spanish MICINN projects nanoTHERM (Grant No. CSD2010-0044) and TAPHOR (Grant No. MAT2012-31392); and the Severo Ochoa Program (MINECO, Grant SEV-2013-0295). M.R.W. acknowledges the postdoctoral Marie Curie Fellowship (IEF) HeatProNano (Grant No. 628197).

* markus.wagner@icn.cat

- [1] M. Kushwaha, P. Halevi, L. Dobrzynski, and B. Djafari-Rouhani, *Physical Review Letters* **71**, 2200 (1993).
- [2] Y. Pennec, J. O. Vasseur, B. Djafari-Rouhani, L. Dobrzynski, and P. A. Deymier, *Surface Science Reports* **65**, 229 (2010).
- [3] T. Still, W. Cheng, M. Retsch, R. Sainidou, J. Wang, U. Jonas, N. Stefanou, and G. Fytas, *Physical Review Letters* **100**, 194301 (2008).
- [4] A. Khelif, Y. Achaoui, S. Benchabane, V. Laude, and B. Aoubiza, *Physical Review B* **81**, 214303 (2010).
- [5] M. Maldovan, *Nature* **503**, 209 (2013).
- [6] A. Khelif, B. Aoubiza, S. Mohammadi, A. Adibi, and V. Laude, *Physical Review E* **74**, 046610 (2006).
- [7] T. Gorishnyy, J. H. Jang, C. Koh, and E. L. Thomas, *Applied Physics Letters* **91**, 20 (2007).

- [8] D. Schneider, F. Liaqat, E. H. El Boudouti, Y. El Hassouani, B. Djafari-Rouhani, W. Tremel, H. J. Butt, and G. Fytas, *Nano Letters* **12**, 3101 (2012).
- [9] B. Graczykowski, M. Sledzinska, N. Kehagias, F. Alzina, J. S. Reparaz, and C. M. Sotomayor Torres, *Applied Physics Letters* **104**, 123108 (2014).
- [10] B. Graczykowski, M. Sledzinska, F. Alzina, J. Gomis-Bresco, J. S. Reparaz, M. R. Wagner, and C. M. Sotomayor Torres, *Physical Review B* **91**, 075414 (2015).
- [11] J. Groenen, F. Poinsothe, A. Zwick, C. M. Sotomayor Torres, M. Prunnila, and J. Ahopelto, *Physical Review B* **77**, 045420 (2008).
- [12] J. Cuffe, E. Chávez, A. Shchepetov, P. O. Chapuis, E. H. El Boudouti, F. Alzina, T. Kehoe, J. Gomis-Bresco, D. Dudek, Y. Pennec, B. Djafari-Rouhani, M. Prunnila, J. Ahopelto, and C. M. Sotomayor Torres, *Nano Letters* **12**, 3569 (2012), arXiv:1209.2324.
- [13] E. Chavez-Angel, J. S. Reparaz, J. Gomis-Bresco, M. R. Wagner, J. Cuffe, B. Graczykowski, A. Shchepetov, M. Prunnila, J. Ahopelto, F. Alzina, and C. M. Sotomayor Torres, *APL Materials* **02**, 012113 (2014).
- [14] J.-K. Yu, S. Mitrovic, D. Tham, J. Varghese, and J. R. Heath, *Nature Nanotechnology* **5**, 718 (2010).
- [15] P. E. Hopkins, C. M. Reinke, M. F. Su, R. H. Olsson, E. a. Shaner, Z. C. Leseman, J. R. Serrano, L. M. Phinney, and I. El-Kady, *Nano Letters* **11**, 107 (2011).
- [16] M. Maldovan, *Physical Review Letters* **110**, 025902 (2013).
- [17] N. Zen, T. Puurtinen, T. J. Isotalo, S. Chaudhuri, and I. J. Maasilta, *Nature communications* **5**, 3435 (2014).
- [18] S. Neogi, J. S. Reparaz, L. F. C. Pereira, B. Graczykowski, M. R. Wagner, M. Sledzinska, A. Shchepetov, M. Prunnila, J. Ahopelto, C. M. Sotomayor-Torres, and D. Donadio, *ACS Nano* **9**, 3820 (2015).
- [19] M. Maldovan, *Nature Materials* **14**, 667 (2015).
- [20] J. Tang, H. T. Wang, D. H. Lee, M. Fardy, Z. Huo, T. P. Russell, and P. Yang, *Nano Letters* **10**, 4279 (2010).
- [21] C. M. Reinke, M. F. Su, B. L. Davis, B. Kim, M. I. Hussein, Z. C. Leseman, R. H. Olsson-Iii, and I. El-Kady, *AIP Advances* **1**, 041403 (2011).
- [22] S. Alaie, D. F. Goettler, M. Su, Z. C. Leseman, C. M. Reinke, and I. El-Kady, *Nature Communications* **6**, 7228 (2015).

- [23] J. Nakagawa, Y. Kage, T. Hori, J. Shiomi, and M. Nomura, *Applied Physics Letters* **107**, 023104 (2015).
- [24] M. Nomura, Y. Kage, J. Nakagawa, T. Hori, J. Maire, J. Shiomi, R. Anufriev, D. Moser, and O. Paul, *Physical Review B* **91**, 205422 (2015).
- [25] R. H. Olsson III and I. El-Kady, *Measurement Science and Technology* **20**, 012002 (2009).
- [26] M. Eichenfield, J. Chan, R. M. Camacho, K. J. Vahala, and O. Painter, *Nature* **462**, 78 (2009).
- [27] A. H. Safavi-Naeini, J. T. Hill, S. Meenehan, J. Chan, S. Gröblacher, and O. Painter, *Physical Review Letters* **112**, 153603 (2014).
- [28] J. Gomis-Bresco, D. Navarro-Urrios, M. Oudich, S. El-Jallal, A. Griol, D. Puerto, E. Chavez, Y. Pennek, B. Djafari-Rouhani, F. Alzina, A. Martínez, and C. Sotomayor Torres, *Nature Communications* **5**, 4452 (2014).
- [29] N. Gomopoulos, D. Maschke, C. Y. Koh, E. L. Thomas, W. Tremel, H. J. Butt, and G. Fytas, *Nano Letters* **10**, 980 (2010).
- [30] A. Sato, Y. Pennek, T. Yanagishita, H. Masuda, W. Knoll, B. Djafari-Rouhani, and G. Fytas, *New Journal of Physics* **14**, 113032 (2012).
- [31] L. C. Parsons and G. T. Andrews, *Journal of Applied Physics* **116**, 033510 (2014).
- [32] S. Mielcarek, A. Trzaskowska, B. Graczykowski, and J. Sarkar, *Physica Status Solidi - Rapid Research Letters* **6**, 175 (2012).
- [33] C. G. Hou, V. L. Zhang, S. C. Ng, M. H. Kuok, H. S. Lim, X. M. Liu, and A. O. Adeyeye, *Applied Physics Letters* **104**, 093108 (2014).
- [34] D. S. Wiersma, *Nature Photonics* **7**, 188 (2013).
- [35] P. W. Anderson, *Physical Review* **109**, 1492 (1958), arXiv:0807.2531.
- [36] T. Schwartz, G. Bartal, S. Fishman, and M. Segev, *Nature* **446**, 52 (2007).
- [37] M. Mascheck, S. Schmidt, M. Silies, T. Yatsui, K. Kitamura, M. Ohtsu, D. Leipold, E. Runge, and C. Lienau, *Nature Photonics* **6**, 293 (2012).
- [38] H. Hu, A. Strybulevych, J. H. Page, S. E. Skipetrov, and B. A. van Tiggelen, *Nature Physics* **4**, 945 (2008), arXiv:0805.1502.
- [39] Z. Yu and S. Fan, *Nature Photonics* **3**, 91 (2009).
- [40] M. Sledzinska, B. Graczykowski, F. Alzina, J. Santiso Lopez, and C. Sotomayor Torres, *Microelectronic Engineering* **149**, 41 (2016).

- [41] A. Bartels, R. Cerna, C. Kistner, A. Thoma, F. Hudert, C. Janke, and T. Dekorsy, *Review of Scientific Instruments* **78**, 035107 (2007).
- [42] F. Hudert, A. Bruchhausen, D. Issenmann, O. Schecker, R. Waitz, A. Erbe, E. Scheer, T. Dekorsy, A. Mlayah, and J. R. Huntzinger, *Physical Review B* **79**, 1 (2009).
- [43] A. Bruchhausen, R. Gebbs, F. Hudert, D. Issenmann, G. Klatt, A. Bartels, O. Schecker, R. Waitz, A. Erbe, E. Scheer, J.-R. Huntzinger, A. Mlayah, and T. Dekorsy, *Phys. Rev. Lett.* **106**, 77401 (2011).
- [44] A. J. Sabbah and D. M. Riffe, *Physical Review B* **66**, 165217 (2002).
- [45] J. J. Letcher, K. Kang, D. G. Cahill, and D. D. Dlott, *Applied Physics Letters* **90**, 2005 (2007).
- [46] C. Thomsen, H. T. Grahn, H. J. Maris, and J. Tauc, *Physical Review B* **34**, 4129 (1986).
- [47] O. B. Wright and V. E. Gusev, *Applied Physics Letters* **66**, 1190 (1995).
- [48] C. M. Sotomayor Torres, A. Zwick, F. Poinsothe, J. Groenen, M. Prunilla, J. Ahopelto, A. Mlayah, and V. Paillard, *Physica Status Solidi C* **1**, 2609 (2004).
- [49] M. Schubert, M. Grossmann, C. He, D. Brick, P. Scheel, O. Ristow, V. Gusev, and T. Dekorsy, *Ultrasonics* **56**, 109 (2014).
- [50] H. J. McSkimin and P. Andreatch, *Journal of Applied Physics* **35**, 2161 (1964).
- [51] J. Cuffe, O. Ristow, E. Chávez, A. Shchepetov, P.-O. Chapuis, F. Alzina, M. Hettich, M. Prunilla, J. Ahopelto, T. Dekorsy, and C. M. Sotomayor Torres, *Physical Review Letters* **110**, 095503 (2013).
- [52] B. C. Daly, K. Kang, Y. Wang, and D. G. Cahill, *Physical Review B* **80**, 174112 (2009).
- [53] J.-Y. Duquesne and B. Perrin, *Physical Review B* **68**, 134205 (2003).
- [54] B. Auld, *Acoustic Fields and Waves in Solids* (Krieger Publishing Company, 1990).
- [55] J. S. Reparaz, E. Chavez-Angel, M. R. Wagner, B. Graczykowski, J. Gomis-Bresco, F. Alzina, and C. M. Sotomayor Torres, *Review of Scientific Instruments* **85**, 034901 (2014).